



HAL
open science

Unexpected Enhanced Reactivity of Aluminized Nanothermites by Accelerated Aging

Tao Wu, Guillaume Lahiner, Christophe Tenailleau, Benjamin Reig, Teresa Hungría, Alain Estève, Carole Rossi

► **To cite this version:**

Tao Wu, Guillaume Lahiner, Christophe Tenailleau, Benjamin Reig, Teresa Hungría, et al.. Unexpected Enhanced Reactivity of Aluminized Nanothermites by Accelerated Aging. *Chemical Engineering Journal*, 2021, 418, pp.129432. 10.1016/j.cej.2021.129432 . hal-03175736

HAL Id: hal-03175736

<https://laas.hal.science/hal-03175736>

Submitted on 21 Mar 2021

HAL is a multi-disciplinary open access archive for the deposit and dissemination of scientific research documents, whether they are published or not. The documents may come from teaching and research institutions in France or abroad, or from public or private research centers.

L'archive ouverte pluridisciplinaire **HAL**, est destinée au dépôt et à la diffusion de documents scientifiques de niveau recherche, publiés ou non, émanant des établissements d'enseignement et de recherche français ou étrangers, des laboratoires publics ou privés.

Unexpected Enhanced Reactivity of Aluminized Nanothermites by Accelerated Aging

*Tao Wu¹, Guillaume Lahiner¹, Christophe Tenailleau², Benjamin Reig¹, Teresa Hungria³,
Alain Esteve¹, Carole Rossi¹*

¹ *LAAS-CNRS, University of Toulouse, 7 Avenue du colonel Roche, 31400 Toulouse, France*

² *CIRIMAT, University of Toulouse, CNRS, UT3-Paul Sabatier, 118 route de Narbonne,
31062 Toulouse, France*

³ *Centre de Microcaractérisation Raimond CASTAING, 3 rue Caroline Aigle, 31400
Toulouse, France*

KEYWORDS: Nanothermites, Aging, DSC, kinetics studies, Friedman isoconventional method, shell-life

Abstract

We examine the thermal aging of four Al based thermites chosen among the most commonly used in microenergetic systems: Al/CuO, Al/Fe₂O₃, Al/Fe₃O₄ and Al/Co₃O₄. For each nanothermite system, we applied the modified Friedmann isoconversional method from DSC signals to calculate the kinetic parameters of reactions and the function of the reaction progress in air and argon. As result, it is found that all thermites should be thermally stable for one century when stored at temperatures below 200 °C, except for Al/Fe₃O₄ which readily converts into Al/Fe₂O₃ before the thermite reaction onset. Then, we designed annealing experiments to a fixed reaction progress : (i) as simulated after 100 years storage at the ambient temperature, (ii) up to 5%. The pressure development and burning rate of aged thermites are compared with

as-prepared ones. After annealing at 200 °C in air and 400 °C in argon, an unforeseen faster reaction and pressurization rates are observed for Al/CuO and Al/Fe₂O₃ thermites. STEM and EDX show that the annealing provokes a modification of the aluminum particles structure accompanied with a softening of the alumina which explains the enhanced pressure performances and burn rates. Whereas the same nanothermites, Al/CuO and Al/Fe₂O₃, annealed at 400 °C in air, feature a reduced reactivity due to the over-oxidations of the aluminum core and the formation of crystalline alumina shell. These results reveal the high complexity of aging processes in powdered nanothermites as it provokes, not only a consumption of the heat reservoir, but also a modification of the Al/oxidizer interface morphology and chemistry which has a greater impact on the material reactivity than cumulative heat release and reaction progress evolution.

1. Introduction

Thermite materials feature redox reactions between a metallic fuel such as aluminum and a metal oxide acting as an oxidizer. They attract a lot of interest as they are known to be stable energetic mixtures possessing high volumetric energy density. [1–4] Traditional thermite composed of particles at the micrometer scale do not manage a fully self-sustained reaction and have, thus, been limited to their original applications such as railroad welding. The development of metallic nanopowders in the last three decades, with regular improvements of their fabrication processes, has permitted the onset of nanothermites [5–11] defined as a metallic fuel/oxidizer mixture in which each component has at least one dimension less than 100 nm. In certain stoichiometric and dimensional conditions, the reaction speeds can be as high as 2500 m/s. [12–14] Consequently, nanothermite mixtures such as Al/CuO, Al/MoO₃, Al/Fe₂O₃, Al/Bi₂O₃, Al/Co₃O₄, *etc.* can replace advantageously other CHNO materials in microscale energetic (or microenergetic) systems [15–27] for applications in civil engineering, and aerospace industry. [28,29]

Despite the active experimental research effort into nanothermites over the three last decades, the literature specifically dedicated to aging studies is notably rare whereas this is a crucial point for their further deployment in current and future applications, not only for safe handling and storage but also to anticipate the aging effects through the design in order to avoid malfunctioning of microenergetic systems incorporating nanothermites. Only two exploratory experimental works [30, 31] showed that aging effects do exist in aluminized nanothermites, but the literature lacks of a rigorous study of the effects of temperature and the ambient air on the thermites' energetic performances. Wang *et al.* [31] experimentally investigated the short-term storage stability of Al/CuO nanothermite prepared by electrospray method, and observed modifications of the mixture performance after 13 months aging at the ambient. They mentioned a slight lowering of the pressure generation from 686 down to 626 kPa, and an increase of the initiation temperature (from 754 to 775 °C) after observing a slight decrease at mid-term aging with further understanding. These observations focusing on a storage of 13 months at the ambient cannot be extended to other thermite couples nor aging conditions. The scope of this present study is to set up a complete study of the thermal aging behavior of four Al based thermites, prepared by nanopowders mixing, chosen among the most used in microenergetic systems: Al/CuO, Al/Fe₂O₃, Al/Fe₃O₄ and Al/Co₃O₄. Their thermite reaction is basically governed by intrinsic properties, characterized by an ensemble of decomposition mechanisms upon heating and driven by kinetic parameters, mass transport processes (diffusion), and thermal properties (specific heat, thermal conductivity). Rigorously, all these kinetic parameters in addition to the physical and thermodynamic parameters governing reaction enthalpies and phase transitions are needed to properly define the function that gives the decomposition progress to predict the aging of nanothermites under different storage temperatures and environmental atmospheres. This is a challenging objective. A traditional and

easier route is to perform a thermokinetic analysis of the material based on differential scanning calorimetry (DSC) experiments with multiple heating rates [32, 33].

Herein, we will carry out a critical study of the application of such a thermokinetic analysis, based on a Friedmann isoconversional method to evaluate the thermal aging of the four aluminized nanothermites, *i.e.* their energetic property changes during storage at various temperature, their shelf life and operative guidelines for achieving virtual thermal aging experiments. After the presentation of the materials preparation and their main energetic properties, the study is divided into two main parts. A first part presents the isoconversional kinetic analysis of DSC data in both air and Ar atmospheres implemented to obtain the variable activation energies of each thermite system, and further predict their lifetime at moderate temperatures (ambient – 300 °C range) in air. Simulations show that, below 200 °C, Al/CuO, Al/Fe₂O₃ and Al/Co₃O₄ are thermally stable hundreds of years, whereas Al/Fe₃O₄ readily starts oxidizing into Fe₂O₃ at 200 °C. The second part aims at investigating how the aging in nanothermites affects their combustion properties. Hence, using predicted kinetic data from the DSC signals, annealing experiments are designed to reach either the reaction progress that would be obtained after 100 years storage at the ambient temperature, or a fixed reaction progress of 5%. Then, the pressure development and burn rate are systematically characterized for aged samples and compared to fresh ones. As unforeseen results, Al/CuO and Al/Fe₂O₃ which underwent mild aging (~15 days at 200 °C, $\alpha \approx 1.1\%$) in air and high temperature aging (~440 °C, 2.6 hours, $\alpha = 5\%$) in argon exhibit higher peak pressure, higher pressurization rates and faster propagation speeds. These results are opposite of traditional data that typically report negative impacts of aging during several months at the ambient or a few days at 200 °C on the thermite reactivity [28, 29, 32]. A careful analysis of structure and phase changes of the nanothermites upon annealing using scanning transmission electron microscopy (STEM) and energy dispersive x-ray analysis (EDX), indicate that the annealing at certain temperatures

and/or environmental conditions enhances the contact between aluminum and metal oxides and modifies the Al nanoparticles structure by softening the alumina shell, which enhances the thermite reactivity.

2. Materials and methods

2.1. Materials

The aluminum nanopowders (Al) (80 nm) were purchased from Novacentrix (Texas, USA) and stored in a glove box. The active Al content was 69% by mass, calculated from thermogravimetric analysis before use. Copper oxide (CuO, ~100 nm), iron oxide (Fe₂O₃, ~50 nm), iron oxide (Fe₃O₄, 50 – 100 nm) and cobalt oxide (Co₃O₄, ~50 nm) purchased from Sigma-Aldrich were directly used as received. Mixtures of different nanothermite materials were prepared using a classic sonication method where Al nanoparticles were mixed with CuO, Fe₂O₃, Fe₃O₄ and Co₃O₄ nanoparticles, respectively, with an equivalence ratio of 1.2 in hexane followed by a 20 minutes sonication. SEM images (**Figure S1**) and XRD patterns (**Figure S2**) of the four starting nanothermite materials (Al/CuO, Al/Fe₂O₃, Al/Fe₃O₄, and Al/Co₃O₄) are given and described in **supplementary file S1**.

2.2. Aging procedure

About 100 mg of each nanothermite material were aged by an isothermal annealing (temperatures are given in section 3.3 after the kinetic analysis) in a furnace under Ar or air (2 L/min gas flow rate). After a natural cooling down to room temperature, the aged materials are collected and stored sealed in a glass vial for future use.

2.3. Characterization methods

For each prepared nanothermite material, the morphology, particle size, agglomeration was observed by SEM using a Hitachi S-4800 (cold FEG) operating at 2.0 kV, and by STEM using a JEOL cold-FEG JEM-ARM200F operated at 200 kV (energy resolution 0.3 eV) and equipped

with a probe Cs corrector with a maximum spatial resolution of 0.078 nm. EDX spectra were recorded with a JEOL CENTURIO SDD detector. The composition and crystallographic structure of the nanothermites was characterized using a SEIFERT XRD 3000 TT XRD with Cu-K α radiation ($\lambda = 1.54059 \text{ \AA}$) fitted with a diffracted-beam graphite monochromator. The diffraction angle (2θ) was scanned from 10 to 100°. Thermal analysis was performed in both argon and air environments at several heating rates (5, 10, 20 and 30 °C/min) by Differential Scanning Calorimetry using a NETZSCH DSC 404 F3 Pegasus device equipped with a DSC-Cp sensor type P over a temperature ranging from ambient to 950 °C. Experiments were performed with ~3 mg of material in platinum crucibles in Ar (99.998% pure) or air atmosphere at a flow rate of 50 mL/min. The traces were normalized by the mass of thermite material and the plotted traces were baseline-corrected by subtracting the signal recorded during a second heating of the same sample. The pressure data were acquired by a high-frequency pressure transducer (Kistler 6215 type) : for all tests, about 13 mg of nanothermite material were packed in a pellet placed in a stainless steel, high pressure resistant cylindrical reactor [20] which has a total volume of 25 mm³ and ignited with a simple NiCr wire. The mean linear burn rate was recorded using a high-speed camera SA3 Photron at a speed of 75,000 frames per second, with a 128 × 32 image resolution [33] : about 25 mg of each materials were loosely deposited in polycarbonate trench (30 mm long, 1 mm wide and 1 mm deep) and ignited at one end.

2.4. Processing of DSC data for kinetics prediction

We used a model-free approach to evaluate the reaction kinetic parameters from the DSC data. The general and effective reaction progress rate equation has the following well-known expression:

$$\frac{d\alpha}{dt} = k_o \exp\left(-\frac{E_a}{RT}\right) \cdot f(\alpha) \quad (1)$$

R being the ideal gas constant, $f(\alpha)$ assumes the type of basic reactive phenomena taking place during the combustion is known. E_a and k_o are the activation energy and pre-factor associated with the thermite reaction, respectively. The most frequently used approach, if several measurements with different heating rates and/or different temperatures ranges are performed, is the method developed by Kissinger [34] assuming the occurrence of first order reactions, i.e. $f(\alpha) = (1 - \alpha)$, limited to independent reactions occurring successively after each other, within specific temperature ranges. However, the thermite reactions, which combines chemical oxido-reduction reactions with mass transport through barrier layers [35-38] that have dynamical changes in their structures over temperature cannot rigorously be reduced to a single Arrhenius law activation. Thus, we opted for the use of a differential isoconversional method based on the Friedmann method. [35, 39-41] In contrast to Kissinger, this methodology states that the reaction rate is only a function of temperature at constant reaction progress. This can be easily demonstrated by taking the logarithmic derivative of the reaction rate equation (Eq. (1)) at α constant.

$$\left[\frac{\partial \ln(d\alpha/dt)}{\partial T^{-1}} \right]_{\alpha} = \left[\frac{\partial \ln k_o(T)}{\partial T^{-1}} \right]_{\alpha} + \left[\frac{\partial \ln f(\alpha)}{\partial T^{-1}} \right]_{\alpha} \quad (2)$$

α being constant, $f(\alpha)$ is also constant, Eq. (2) becomes:

$$\left[\frac{\partial \ln(d\alpha/dt)}{\partial T^{-1}} \right]_{\alpha} = - \frac{E_a}{R} \quad (3)$$

Thus, the temperature dependence of the isoconversional rate can be used to evaluate isoconversional values of the activation energy, E_a , which are now defined at each point of the reaction progress, without assuming any particular form of the reaction model. [38] Concretely, for each prepared nanothermite material, a set of DSC experiments were conducted in both argon and air at 5, 10, 20, 30 °C/min in the temperature range of ambient - 950 °C. DSC data are presented and analyzed in **supplementary file S2**. It has to be noted that because the temperature ranges used in the experiments are broad (20 - 950 °C), the baselines are not linear.

Therefore, to reconstruct an accurate temperature dependent baseline, it was assumed that the degree of conversion was the similar for all heating rates when the first and strongest peak occurred in the DSC signals. The initial and final slopes of the DSC curve recorded at 10 °C/min were used to construct a smooth initial baseline for this measurement and determine the respective degree of conversion corresponding to the position of the first peak. This degree of conversion corresponded to 5%, and it was used consistently to adjust the baseline representing the weighted averages of the initial and final slopes for other used heating rates.

3. Results

3.1. Thermal analysis and kinetic parameters of as-prepared thermite materials

Figure 1 shows the DSC traces of the four nanothermite materials, Al/CuO, Al/Fe₂O₃, Al/Fe₃O₄ and Al/Co₃O₄, collected at a heating rate of 10 °C/min in Ar (**Figure 1a**) and air (**Figure 1b**). To be noted, the heat flow values on Y axis are offset here (See **Figure S3** for non-offset curves). The DSC result of pure Al is also shown in Figure S4. For all nanothermite systems two main exothermic peaks (upward peaks) are observed: first one occurs prior to the melting of Al, in a range of 550 - 600 °C and the second, less intense and broader, occurs in the range of 700 - 950 °C. The endothermic peak at ~660 °C corresponds to the aluminum core melting as all systems are prepared in fuel rich condition (1.2 stoichiometry). It is interesting to note that temperatures at which the first exothermic peaks occur are comparable for the four materials systems: ~525 °C and ~575 °C, for the onset (T_{onset}) and peak temperature (T_{peak}) respectively. This indicates that these four thermite materials, when being heated to 600 °C undergo a similar thermal decomposition pathways based on solid-state transport mechanisms : oxygen diffusion [22] and counter diffusion of Al ions through alumina shell [41]. In addition, both Al/iron oxides (Al/Fe₂O₃ and Al/Fe₃O₄) feature the less intense first exotherm which agrees with their higher decomposition temperatures (compared to other considered oxidizers)

together with their high activation barrier for oxygen diffusion [42, 43]. This is also consistent with the fact that iron oxides are often used as moderators (weak oxidizer) to reduce the reactivity and sensitivity of other nanothermites [21, 41]. It is also to be noted that the Al melting endotherm is more intense in Al/iron oxide materials, which indicates that less aluminum is being consumed by the oxides before its melting compare to the two others, CuO and Co_3O_4 .

For each thermite systems, the heat release, ΔH_{exp} , is calculated by integrating the DSC traces over a temperature range from 400 to 950 °C (**Table 1** and **Table 2**). It is important to mention that while the exothermicity can be detected reliably at defined temperatures and relative peak sizes can be compared, an absolute and unambiguous value of heat release cannot be reported with accuracy. Despite this fact, the heat release, ΔH_{exp} is an important metric often used to qualitatively compare energetic performance of different thermite couples. From the highest to the lowest ΔH_{exp} , the ranking is Al/CuO, Al/ Fe_2O_3 , Al/ Fe_3O_4 , Al/ Co_3O_4 . Al/CuO nanothermite demonstrates the highest heat release closed to its theoretical one (4 kJ/g), whereas Al/ Co_3O_4 material releases only 58% of its theoretical potential (~4 kJ/g). Al/ Fe_2O_3 and Al/ Fe_3O_4 materials release only 70% and 68% of their theoretical values, respectively. Sintering process that may happen upon heating iron and cobalt oxides [21, 22] can explain why ΔH_{exp} is well below the theoretical values for Al/ Fe_2O_3 , Al/ Fe_3O_4 and Al/ Co_3O_4 materials. Indeed, sintering process traps the oxygen inside leading to a long period of oxygen releasing time and therefore limiting the exothermicity of iron oxides and cobalt oxides-based nanothermites [17]. Jian *et al.* also reported that the ignition temperature of Al/ Co_3O_4 is 400 °C higher than the oxygen release temperature of Co_3O_4 , which to some extent implies the redox reaction between Al and Co_3O_4 is much harder to initiate and the oxygen release from Co_3O_4 is much less effective than CuO [22].

Another observation from the DSC traces is that the environment, being oxidizing or inert, does not impact the onset of reactions: temperatures at which the first exothermic peaks occur are similar in air and in Ar for all four nanothermite materials (**Table 1** and **Table 2**). This indicates that the condensed phase still plays the dominant role in this first reactional step. However, the presence of oxygen in the environment enhances the heat released in the first exotherm: for all material systems, we note that the energy released before 600 °C is much greater in air than in argon (see **Table 1** and **Table 2**). ΔH_{exp} prior Al melting is increased by ~1.4, ~1.6 and ~4 for Al/CuO, Al/Co₃O₄ and Al/iron oxides cases, respectively. We deduce that ambient molecular oxygen contributes to the thermite reaction in all cases, and greatly when for iron oxides as they are poor oxygen providers at this temperature range. Besides, the endotherm peaks at 660 °C for all four nanothermites in oxidizing air are weaker than those in inert argon atmosphere which is in accordance with precedent comment: more aluminum is being consumed during the first exothermic step due to the presence of gaseous O₂ in air.

Now, looking further at the Al/Co₃O₄ thermite case, unlike the three other thermites, the atmospheric environment does not change the aluminum melting endotherm intensity/area. This means that the same amount of aluminum core is consumed in the first exothermic event in either inert or oxidizing environment. Al/Co₃O₄ powders annealed at 635 and 890 °C in air and Ar at 10 °C/min were analyzed by XRD (**Figure S5**) to determine their phases prior and after Al melting. Even though the characteristic peaks of aluminum are overlapped with those of Co₃O₄, the intensities of aluminum peaks are greatly reduced in the product collected at 635 °C (Al peak at 2θ 83° disappeared) indicating that some aluminum was consumed, which is also asserted by the increase in the heat release upon air exposure. Since the characteristic XRD peaks (2θ 10 – 100°) of Co₃O₄ and Al₂CoO₄ are overlapped, it is difficult to firmly determine the phases of the sample annealed at 890 °C. However, we highly suspect that the majority of cobalt elements is present in Al₂CoO₄ in these two annealed samples, where some aluminum is

trapped during the first exothermic event and thus leading to the inefficiency of Al/Co₃O₄ thermite reaction (Al/Co₃O₄ thermite releases only 58% of its theoretical total heat). Also, it could also explain why under air exposure, the heat release is increased by a factor of 1.6 suggesting a re-oxidation of reduced cobalt by the air, rather than oxidation of the aluminum reservoir.

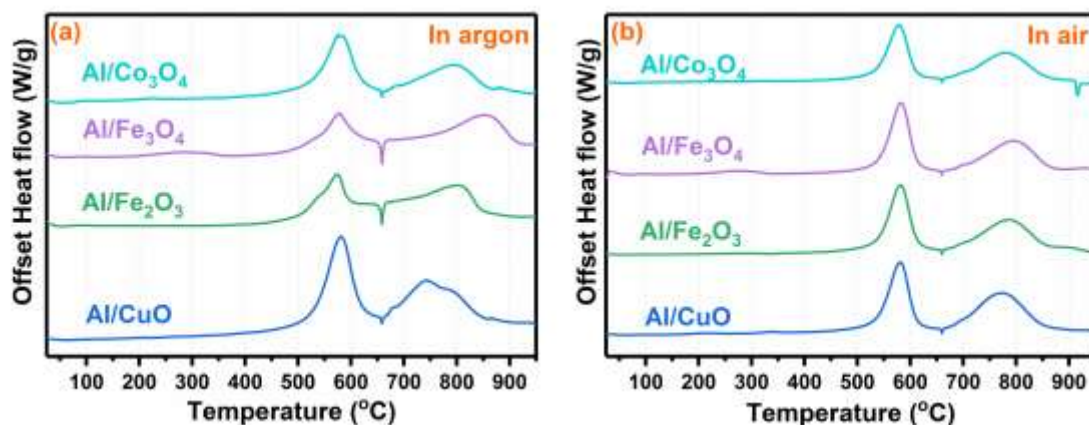


Figure 1. DSC traces collected for Al/CuO, Al/Fe₂O₃, Al/Fe₃O₄ and Al/Co₃O₄ as prepared and ramped in flowing Ar (a) and air (b) at 10 °C/min. The y-axis values are offset.

Table 1. Onset temperature, peak temperature and heat released collected for Al/CuO, Al/Fe₂O₃, Al/Fe₃O₄ and Al/Co₃O₄ systems in Ar environment.

Material system	T_{onset} (°C)		T_{peak} (°C)		Heat released ΔH_{exp} (J/g)			
	1 st exotherm	2 nd exotherm	1 st exotherm	2 nd exotherm	Total	Theoretical total [1]	1 st exotherm	Endotherm
Al/CuO	528	691	581	743	3945	4072	1567	26
Al/Fe ₂ O ₃	514	733	575	701	2791	3956	470	47
Al/Fe ₃ O ₄	527	770	578	853	2516	3677	580	51
Al/Co ₃ O ₄	534	698	575	794	2457	4234	1063	8

Table 2. Onset temperature, peak temperature and heat released collected for Al/CuO, Al/Fe₂O₃, Al/Fe₃O₄ and Al/Co₃O₄ systems in air environment.

Material system	T_{onset} (°C)		T_{peak} (°C)		Heat released ΔH_{exp} (J/g)			
	1 st exotherm	2 nd exotherm	1 st exotherm	2 nd exotherm	Total ΔH_{exp} (J/g)	Theoretical total (J/g) [1]	1 st exotherm	Endotherm
Al/CuO	538	697	581	772	5125	4072	2241	17
Al/Fe ₂ O ₃	539	705	581	785	4214	3956	2114	11
Al/Fe ₃ O ₄	540	710	583	796	4302	3677	2217	11
Al/Co ₃ O ₄	536	702	579	780	3958	4234	1756	10

The data collected from DSC experiments at various heating rates (see **Figure S6-7**) were then processed in order to plot the dependence of the activation energy against the reaction progress or cumulative heat release (**Figure 2**) in air and argon environment. In argon, the dependency of activation energy on the reaction progress indicates, for Al/CuO, Al/Fe₂O₃ and Al/Co₃O₄ nanothermite materials, a large plateau confirming that the exothermic events are dominated by a single activated process. The value of the activation energy remains close to 200, 150, and 200 kJ/mol until a reaction progress of about 25%, for Al/CuO, Al/Fe₂O₃, and Al/Co₃O₄ respectively. However, the activation energy is not constant for Fe₃O₄ oxidizer: we distinguish two values for Al/Fe₃O₄, 65 and 200 kJ/mol. The first exothermic peak could be deconvoluted into three main contributions, which results in the splitting of the activation barrier into two well stabilized parts: a first plateau is obtained at about 65 kJ/mol, while a second portion stabilizes in the range of 180 - 230 kJ/mol. This might correspond to the two remaining DSC

peak contributions. In contrast, in air, all DSC peaks (**Figure S7**) appear sharper and exhibit a single plateau as seen in **Figure 2**, even in the case of Al/Fe₃O₄ material. The activation energy is around 250 kJ/mol until a reaction progress reaches ~40%, for Al/CuO, Al/Fe₂O₃, Al/Fe₃O₄, and Al/Co₃O₄ respectively.

Despite the same temperature range, the reaction progress doubles when in air which clearly points to the role of the atmosphere at low heating ramp, which leads to faster and higher degree of the energy reservoir consumption.

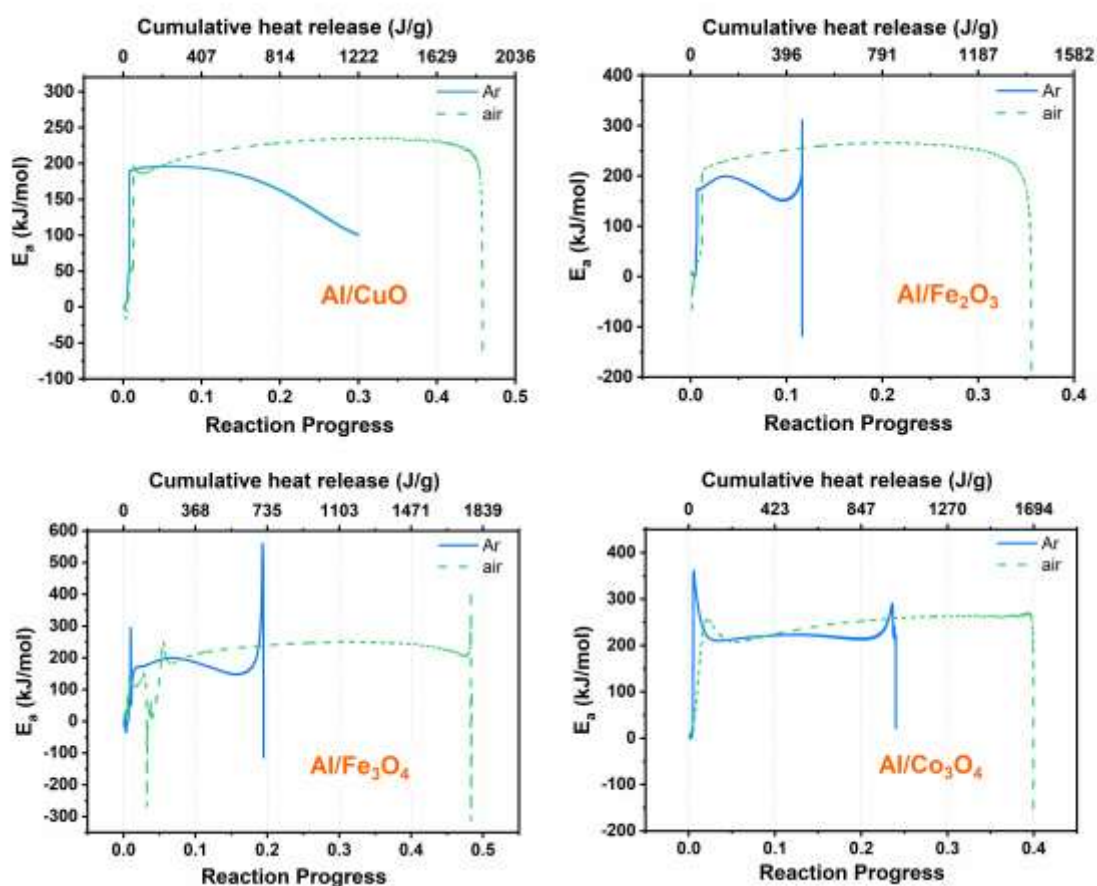


Figure 2. Activation energy (kJ/mol) of Al/CuO, Al/Fe₂O₃, Al/Fe₃O₄ and Al/Co₃O₄ in Ar (solid line) and in Air (dashed line) as a function of reaction progress and cumulative heat release.

3.2. Prediction of heat released under isothermal conditions

The above kinetic parameters allow us to simulate systematically the behavior of each nanothermite materials in terms of the reaction progress and cumulative heat release over time and under isothermal conditions (**Figure 3**). For all four nanothermite materials, there are less than 1.2% of energy lost after 100 years at temperatures below 200 °C, except for Al/Fe₃O₄, where Fe₃O₄ oxidizes into Fe₂O₃ after several hours at 200 °C, and then follows the similar reactional pathway as to Al/Fe₂O₃. We can conclude that the aluminized thermites except Al/Fe₃O₄, are thermally stable materials at the ambient and low temperature (< 200 °C). The only physicochemical process that is activated at low temperature does penalize only a negligible part of the energetic reservoir.

Figure 3 shows that an aging step is reached at 300 °C. After one-year storage at such temperature, cumulative heat release reaches 300 ($\alpha = 7\%$), 92 ($\alpha = 2\%$), 225 ($\alpha = 6\%$), 80 J/g ($\alpha = 2\%$) for Al/CuO, Al/Fe₂O₃, Al/Fe₃O₄ and Al/Co₃O₄ respectively. After ten-years storage at 300 °C, cumulative heat release increases up to 850 ($\alpha = 21\%$), 265 ($\alpha = 7\%$), 700 ($\alpha = 19\%$), and 300 J/g ($\alpha = 7\%$) for Al/CuO, Al/Fe₂O₃, Al/Fe₃O₄ and Al/Co₃O₄ respectively, which now represents a significant reaction advancement.

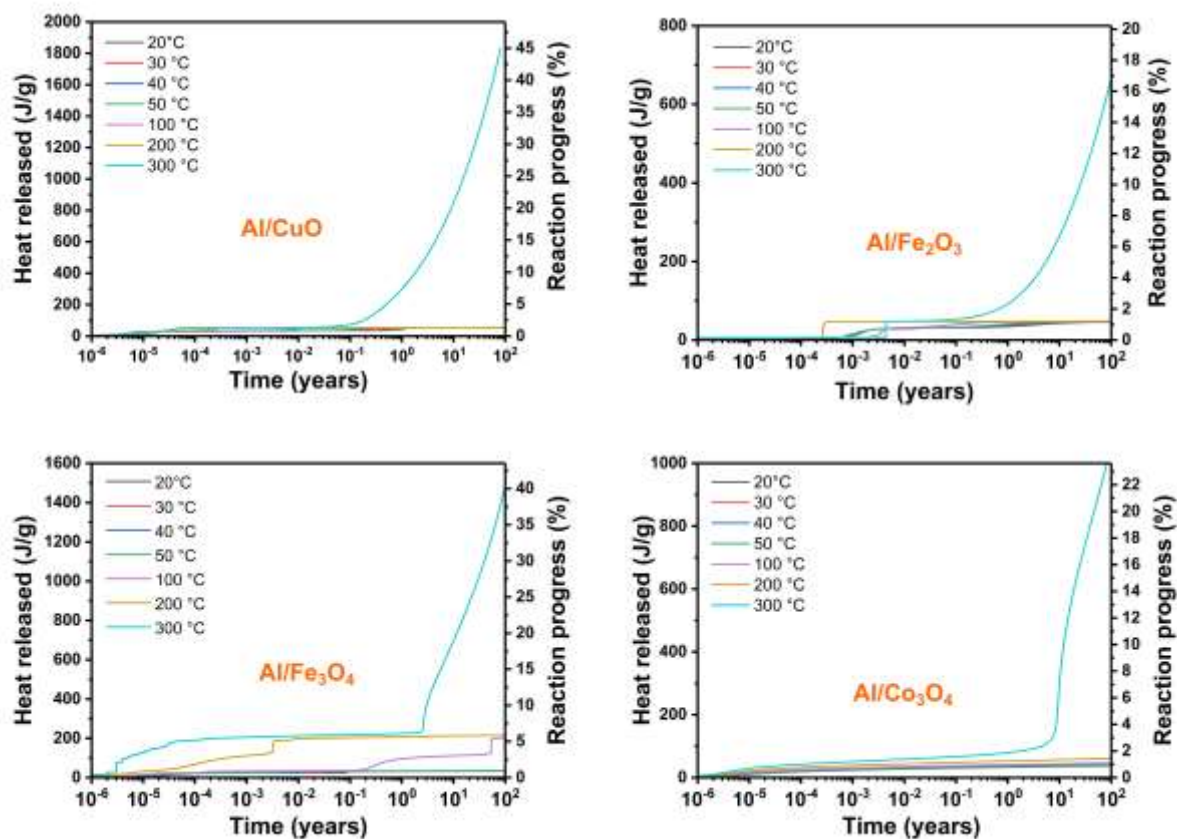


Figure 3. Simulated heat release and reaction progress of each nanothermite system at various temperatures (20, 30, 40, 50, 100, 200, and 300 °C) in air.

3.3. *Impact of thermal aging on reactivity and combustion performances*

This section aims at investigating how the aging in nanothermites affects their combustion properties. Accelerated aging *i.e.* annealing experiments, were carried out to simulate various aging conditions, and the combustion performance and reactivity change of the aged thermites were quantified in terms of linear burn rate, peak pressure and pressurization rate within a closed chamber.

From the kinetics parameters plotted in **Figure 2**, we calculated the annealing temperature-time couples in order to:

1. Obtain an equivalent aging of nanothermites for a 100-years storage under ambient condition, *i.e.* a reaction progress α equal to 1.2% for Al/CuO, 1.1% Al/Fe₂O₃, 5.5% Al/Fe₃O₄ and 1% Al/Co₃O₄. To achieve such reaction progresses, each nanothermite was annealed at 200 °C in air for ~15 days (according to predictions in **Figure 3**).
2. Achieve a reaction progress of 5% which corresponds to a heat release of 204, 198, 184 and 212 J/g for Al/CuO, Al/Fe₂O₃, Al/Fe₃O₄ and Al/Co₃O₄, respectively. Fixing the annealing time at 2.6 h, the corresponding annealing temperature was calculated from the thermokinetic analysis, and summarized in **Table 3**.

Table 3. Corresponding annealing temperature to obtain 5% of reaction progress after 2.6 hours for each nanothermite in argon and air.

Nanothermite material	Calculated annealing temperature (°C)	
	In Ar	In air
Al/CuO	400	425
Al/Fe ₂ O ₃	430	430
Al/Fe ₃ O ₄	450	320
Al/Co ₃ O ₄	450	440

To make the discussion easier, the labelling of the four materials under different aging conditions goes as the following, taking Al/CuO for example: Al/CuO^{ref}, Al/CuO^{200C_{air}}, Al/CuO^{400C_{argon}}, and Al/CuO^{425C_{air}}, refer to as the Al/CuO nanothermite as-prepared, annealed ~15 days at 200 °C, annealed 2.6 h at temperature value reported in the **Table 3** in Ar and in air, respectively. The same labeling rule was applied to Al/Fe₂O₃, Al/Fe₃O₄ and Al/Co₃O₄ as well.

Table 4 presents the close bomb tests results (peak pressure, pressurization rate) and linear burn rates for the four nanothermite couples after the different aging conditions and compared with as-prepared materials (fresh samples). The pressure traces and high-speed video images of the combustion of all samples tested are provided in **Figure 4** and **Figure S8**, and **Figure S9**, respectively.

Table 4. Results of peak pressure, pressurization rate and burn rate for Al/CuO, Al/Fe₂O₃, Al/Fe₃O₄ and Al/Co₃O₄ nanothermites (average value and deviation when possible are calculated on 3 experiments for each sample).

Samples		Peak pressure (kPa)	Pressurization rate (kPa/ μ s)	Burn rate (m/s)
Al/CuO	Al/CuO ^{ref}	700 \pm 100	5400 \pm 2700	40 \pm 2
	Al/CuO ^{200C_{air}}	600 \pm 10	18900 \pm 7200	100 \pm 5
	Al/CuO ^{400C_{argon}}	600 \pm 100	9000 \pm 4100	75 \pm 5
	Al/CuO ^{425C_{air}}	300 \pm 10	4200 \pm 400	30 \pm 2
Al/Fe ₂ O ₃	Al/Fe ₂ O ₃ ^{ref}	50 \pm 10	20 \pm 2	0.4 \pm 0.1
	Al/Fe ₂ O ₃ ^{200C_{air}}	90 \pm 20	170 \pm 10	0.6 \pm 0.2
	Al/Fe ₂ O ₃ ^{430C_{argon}}	30 \pm 10	10 \pm 2	0.3 \pm 0.1
	Al/Fe ₂ O ₃ ^{430C_{air}}	20 \pm 10	10 \pm 2	0.2 \pm 0.1
Al/Fe ₃ O ₄	Al/Fe ₃ O ₄ ^{ref}	2	2	No propagation
	Al/Fe ₃ O ₄ ^{200C_{air}}	10	10	
	Al/Fe ₃ O ₄ ^{450C_{argon}}	10	10	
	Al/Fe ₃ O ₄ ^{320C_{air}}	30	30	
Al/Co ₃ O ₄	Al/Co ₃ O ₄ ^{ref}	10	10	

	Al/Co ₃ O ₄ ^{200C_air}	20	20	
	Al/Co ₃ O ₄ ^{450C_argon}	No ignition		
	Al/Co ₃ O ₄ ^{440C_air}			

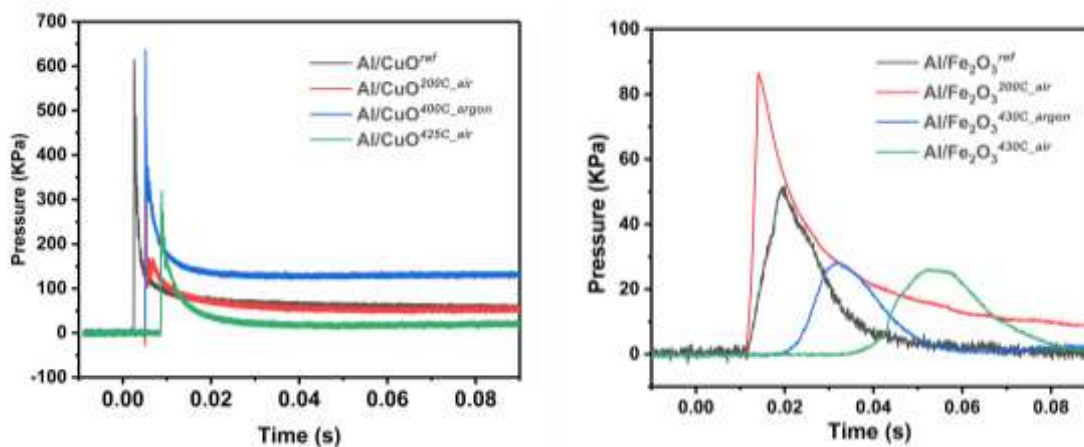


Figure 4. Pressure vs time for Al/CuO (left) and Al/Fe₂O₃ (right) under different conditions, Reference; Annealed at 200 °C for 15 days; Aged in argon; Aged in air. Results of Al/Fe₃O₄ and Al/Co₃O₄ are provided in **Figure S8**.

Al/Fe₃O₄ and Al/Co₃O₄ do not produce much pressure, which was expected as they are known to exhibit gasless combustion. Consistently, it has to be noted that large spherical metal (Fe and Co) balls (~500 μm to 1 mm) were collected from the closed bomb chamber after the tests indicating that the combustion occurs in the condensed phase. Both pressurization and pressure values are small, in addition to what none of them featured sustained combustion. Even the reference samples do not sustain propagation, so that discussing the effect of aging on their performances is not relevant. Another worth mentioning point is that the color of Al/Fe₃O₄ powder changed from black to red after aging and XRD analysis (**Figure S10**) indicated an oxygen state shifted from Fe₃O₄ to Fe₂O₃.

For Al/CuO thermite, the measured peak pressure values do not vary much comparing with the as prepared material, after aging at 200 °C in air or ~400 °C in argon (**Table 4**, peak pressure values in 600 – 700 kPa range for Al/CuO^{ref}, Al/CuO^{200C_{air}} and Al/CuO^{400C_{argon}}). Whereas the peak pressure reduces by 50% after aging at high temperature in air (Al/CuO^{425C_{air}}) which demonstrates that air plays a part in reducing its pressure generation performance. Surprisingly, the highest pressurization rate ($\sim 2 \times 10^4$ kPa/ μ s) among all four Al/CuO samples is generated by the Al/CuO nanothermite being annealed in air at 200 °C for ~15 days. Then, the second highest value is generated by Al/CuO^{400C_{argon}} with $\sim 1 \times 10^4$ kPa/ μ s roughly the double compared to Al/CuO^{ref} ($\sim 5.5 \times 10^4$ kPa/ μ s). Therefore, the annealing at 200 °C in air and at ~400 °C in argon have both a beneficial effect on the Al/CuO reactivity and combustion performance (see discussion section).

For Al/Fe₂O₃, both peak pressure and pressurization rate values (**Table 4**) are much smaller than those of Al/CuO (50 vs 700 kPa and 20 vs 5400 kPa/ μ s) in agreement with the previous studies on these two nanothermite materials [43, 44]. Among the four Al/Fe₂O₃ samples, Al/Fe₂O₃^{200C_{air}}, annealed at 200 °C, features the highest peak pressure and pressurization rate values, 90 kPa and 170 kPa/ μ s respectively, against 50 kPa and 20 kPa/ μ s obtained for Al/Fe₂O₃^{ref}. The Al/Fe₂O₃ sample annealed at 430 °C temperature in air (Al/Fe₂O₃^{430C_{air}}) features the lowest peak pressure (20 kPa) and pressurization rate values (10 kPa/ μ s). Unlike Al/CuO, the pressurization rate of Al/Fe₂O₃ is also weakened after being aged at high temperature in an inert environment (Al/Fe₂O₃^{430C_{argon}}).

In agreement with the pressure development results, the burn rate (**Table 4**, last column) is increased by a factor ~2 to reach 100 and 75 m/s when Al/CuO is annealed in air at 200 °C for ~15 days and in Argon at ~400°C for 2.6 h, respectively. Although the burn rates from Al/Fe₂O₃ samples are significantly slower than those of Al/CuO, the same trend is found: the annealing at 200 °C in air and at ~435 °C in argon induces a beneficial effect.

4. Discussion

The peak pressure and pressurization rate values are higher in the Al/CuO (and a lesser extent Al/Fe₂O₃) thermites annealed ~15 days at 200 °C in air or 2.6 h at ~400 °C in Ar compared to fresh ones. Since the difference among the combustion data from Al/Fe₂O₃ samples are not significant enough to draw strong arguments, we focus now on Al/CuO cases to further understand the mechanisms at play in these observations. TEM and EDX were performed on Al/CuO^{ref}, Al/CuO^{200C_{air}} and Al/CuO^{425C_{air}} samples (**Figure 5**) in order to identify changes in the structure and composition upon aging. Al/CuO^{425C_{air}} is not included here because it does not demonstrate an improving effect as strong as to Al/CuO^{200C_{air}} and thus diminished its importance in this study.

In all the TEM images of **Figure 5**, particles with darker color and irregular shapes are CuO nanoparticles whereas spherical particles with lighter color are aluminum ones. For Al/CuO^{ref}, both aluminum and CuO nanoparticles are aggregated within their own clusters and then align together to create the contact between fuel and oxide particles. Both TEM and EDX analysis show uniform and flawless amorphous alumina shell in surrounding aluminum nanoparticle cores, with a thickness of 4.5 ± 0.8 nm (**Figure 5d-e**, thicknesses are measured by ImageJ). After annealing at 200 °C, referred to as Al/CuO^{200C_{air}}, the mixing between Al and CuO is improved compared to Al/CuO^{ref} since the majority of aluminum nanoparticles examined are in contact to CuO nanoparticles (**Figure 5g-k**), which is not the case for Al/CuO^{ref}. We also clearly observe in the TEM images of Al/CuO^{200C_{air}} (**Figure 5i-k**), that the alumina shell is now ill-defined and features non-uniform shapes; the outside alumina shell appears to be in jagged shapes with different thicknesses (2.5 - 10 nm) around the aluminum core. This inhomogeneity in thickness and shape may be the reason for a higher rate of mass transport of species across the shell, leading to the increase in reactivity. From these observations, we suggest that, upon Al melting, a better oxidizer wetting process is achieved, that may explain

this unforeseen faster reaction rate after annealing despite the reduction of the energy reservoir. A similar phenomenon was reported by Jacob *et al.* [45] where they argued that a soften effect on the shell from pre-annealing of the aluminum could lead to faster release of aluminum. Thus, the improved reactivity of $\text{Al/CuO}^{200\text{C}_{air}}$ results from these two beneficial effects.

Looking now at powders annealed in air at 425 °C, referred to as $\text{Al/CuO}^{425\text{C}_{air}}$, we observe a better contact between Al and CuO than in Al/CuO^{ref} (**Figure 5m-q**). However, the alumina shell thickened up to ~50 nm (**Figure 5r**). In certain TEM images (**Figure 5o-q**), we can also observe some alumina shells being peeled off from the aluminum nanoparticles (marked by red arrows), exposing the core to air that leads to further oxidation of the aluminum. Even though such alumina pilling phenomenon was also found in $\text{Al/CuO}^{200\text{C}_{air}}$ (**Figure 4j**), it is much severe for $\text{Al/CuO}^{425\text{C}_{air}}$ since there are way more alumina scattered around the aluminum particles especially in **Figure 5o and 5q**. The EDX analysis in **Figure 5r** also shows significant oxidation of the aluminum nanoparticles, which might explain the reduced combustion performance. At some place, the alumina shell also shows crystalline structures (marked by arrows in **Figure 5q**). Previous studies have shown that transitioning from amorphous to crystalline alumina shell in Al-based energetic materials can reduce their flame propagation speeds by as much as 45% depending on the sizes of aluminum [46]. The reduction of combustion performances of $\text{Al/CuO}^{425\text{C}_{air}}$ is therefore attributed to the thickening, and presumably difference in the alumina structure alumina (shell transitions from amorphous to crystalline), as well as the consumption of the aluminum reservoir.

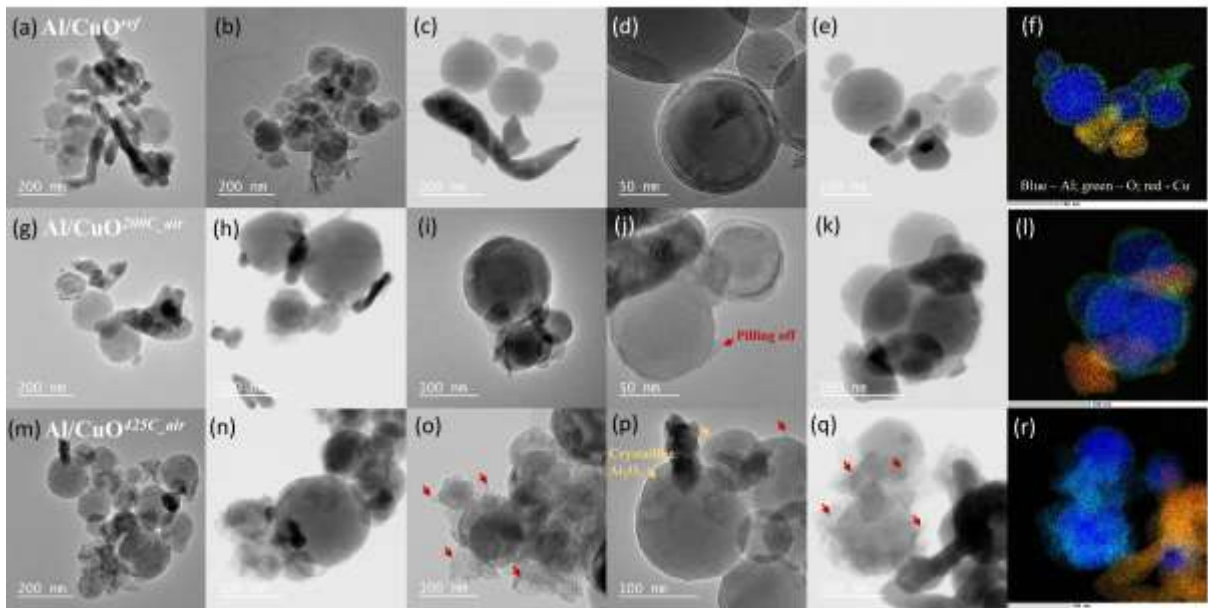


Figure 5. TEM images and EDX mapping results of Al/CuO^{ref} (a-f), Al/CuO^{200C_{air}} (g-l) and Al/CuO^{425C_{air}} (m-r).

5. Conclusions

We evaluated a modified Friedman isoconventional method as a tool to predict the shelf life of four nanothermite mixtures (Al/CuO, Al/Fe₂O₃, Al/Fe₃O₄ and Al/Co₃O₄) at the ambient temperature and operate virtual thermal aging. Unexpectedly, results show that certain aging conditions can boost the combustion performance while sacrificing portion of the energetic reservoir. Another message drawn from these results is that when considering nanothermite materials, contrary to CHNO energetics, aging is not only a matter of the energetic reservoir consumption. It may provoke a modification of the reactant structures accompanied with a modification of the Al/oxidizer interface chemistry which has a greater impact on the material reactivity than cumulative heat release and reaction progress evolution. Obviously, caution must be taken, due to many assumptions associated with the isoconventional methods, but even more from the subtle low temperature aging mechanisms that do not leave an exploitable thermal signature in the DSC traces. Therefore, thermokinetic study must be combined with a precise evaluation of morphological and structural changes at the nanoscale in the nanothermites

upon heating as it was recently proposed for nanolaminate systems [36, 38]. Such an approach would make it possible to identify the main reactional steps of low temperature, as recorded in the DSC but without any *a priori* knowledge of their fundamentals.

Author contributions

T. W. prepared all samples, performed all characterization measurements, and drafted the manuscript. G.L. assisted T. W. in aging predictions. C. T. performed XRD measurements. B. R. assisted T.W. in DSC experiments. T. H. performed all TEM observations and EDX analysis. A.E and C.R. provided support for the manuscript preparation. C.R. supervised this research.

Funding Sources

C.R. received funding from the European Research Council (ERC) under the European Union's Horizon 2020 research and innovation program (grant agreement No. 832889 - PyroSafe).

Competing financial interests

The authors declare no competing financial interests.

Acknowledgment

The authors acknowledge support from the European Research Council (H2020 Excellent Science) Researcher Award (grant 832889 – PyroSafe) and the Occitanie Region / European Union for their FEDER support (THERMIE grant). We thank as well Sandrine Assie-Souleille for her great support with experimental set up.

Supplementary materials

Supplementary materials associated with this article are available in a separate document.

Reference

- [1] S.H. Fischer, M.C. Grubelich, Theoretical energy release of thermites, intermetallics, and combustible metals, in: Monterey, CA, USA, 1998. <https://doi.org/10.2172/658208>.
- [2] C. Rossi, Engineering of Al/CuO reactive multilayer thin films for tunable initiation and actuation, *Propell Explos Pyrot* 44 (2019) 94-108. <https://doi.org/10.1002/prop.201800045>.
- [3] E.C. Koch, S. Knapp, Thermites - Versatile Materials, *Propell Explos Pyrot* 44 (2019) 7-7. <https://doi.org/10.1002/prop.201980131>.
- [4] C. Rossi, K. Zhang, D. Esteve, P. Alphonse, P. Tailhades, C. Vahlas, Nanoenergetic materials for MEMS: A review, *J Microelectromech S* 16 (2007) 919-931. <https://doi.org/10.1109/Jmems.2007.893519>.
- [5] C.E. Aumann, G.L. Skofronick, J.A. Martin, Oxidation Behavior of Aluminum Nanopowders, *J Vac Sci Technol B* 13 (1995) 1178-1183. <https://doi.org/10.1116/1.588232>
- [6] A. Chaalane, C. Rossi, D. Esteve, The formulation and testing of new solid propellant mixture (DB plus x%BP) for a new MEMS-based microthruster, *Sensor Actuat a-Phys* 138 (2007) 161-166. <https://doi.org/10.1016/j.sna.2007.04.029>.
- [7] E.L. Dreizin, Metal-based reactive nanomaterials, *Prog Energ Combust* 35 (2009) 141-167. <https://doi.org/10.1016/j.pecs.2008.09.001>.
- [8] R.A. Yetter, G.A. Risha, S.F. Son, Metal particle combustion and nanotechnology, *P Combust Inst* 32 (2009) 1819-1838. <https://doi.org/10.1016/j.proci.2008.08.013>.
- [9] K.S. Martirosyan, Nanoenergetic Gas-Generators: principles and applications, *J Mater Chem* 21 (2011) 9400-9405. <https://doi.org/10.1039/C1jm11300c>.
- [10] C. Rossi, A. Esteve, P. Vashishta, Nanoscale energetic materials, *J Phys Chem Solids* 71 (2010) 57-58. <https://doi.org/10.1016/j.jpcs.2009.10.015>.

- [11] T. Wu, X.Z. Wang, P.Y. Zavalij, J.B. DeLisio, H.Y. Wang, M.R. Zachariah, Performance of iodine oxides/iodic acids as oxidizers in thermite systems, *Combust Flame* 191 (2018) 335-342. <https://doi.org/10.1016/j.combustflame.2018.01.017>.
- [12] K.S. Martirosyan, L. Wang, D. Luss, Novel nanoenergetic system based on iodine pentoxide, *Chem Phys Lett* 483 (2009) 107-110. <https://doi.org/10.1016/j.cplett.2009.10.038>.
- [13] K.S. Martirosyan, L. Wang, A. Vicent, D. Luss, Synthesis and performance of bismuth trioxide nanoparticles for high energy gas generator use, *Nanotechnology* 20 (2009). <https://doi.org/10.1088/0957-4484/20/40/405609>.
- [14] J.L. Cheng, H.H. Hng, Y.W. Lee, S.W. Du, N.N. Thadhani, Kinetic study of thermal- and impact-initiated reactions in Al-Fe₂O₃ nanothermite, *Combust Flame* 157 (2010) 2241-2249. <https://doi.org/10.1016/j.combustflame.2010.07.012>.
- [15] D. Stamatis, E.L. Dreizin, K. Higa, Thermal Initiation of Al-MoO₃ Nanocomposite Materials Prepared by Different Methods, *J Propul Power* 27 (2011) 1079-1087. <https://doi.org/10.2514/1.B34179>.
- [16] C. Rossi, B. Larangot, P.Q. Pham, D. Briand, N.F. de Rooij, M. Puig-Vidal, J. Samitier, Solid propellant microthrusters on silicon: Design, modeling, fabrication, and testing, *J Microelectromech S* 15 (2006) 1805-1815. <https://doi.org/10.1109/Jmems.2006.880232>.
- [17] H. Pezous, C. Rossi, M. Sanchez, F. Mathieu, X. Dollat, S. Charlot, V. Conedera, Fabrication, assembly and tests of a MEMS-based safe, arm and fire device, *J Phys Chem Solids* 71 (2010) 75-79. <https://doi.org/10.1016/j.jpics.2009.08.018>.
- [18] A. Nicollet, G. Lahiner, A. Belisario, S. Souleille, M. Djafari-Rouhani, A. Esteve, C. Rossi, Investigation of Al/CuO multilayered thermite ignition, *J Appl Phys* 121 (2017). <https://doi.org/10.1063/1.4974288>.

- [19] D. Sundaram, V. Yang, R.A. Yetter, Metal-based nanoenergetic materials: Synthesis, properties, and applications, *Prog Energ Combust* 61 (2017) 293-365. <https://doi.org/10.1016/j.pecs.2017.02.002>.
- [20] X.Z. Wang, W.B. Zhou, J.B. DeLisio, G.C. Egan, M.R. Zachariah, Doped delta-bismuth oxides to investigate oxygen ion transport as a metric for condensed phase thermite ignition, *Phys Chem Chem Phys* 19 (2017) 12749-12758. <https://doi.org/10.1039/c6cp08532f>.
- [21] K.T. Sullivan, N.W. Piekielek, C. Wu, S. Chowdhury, S.T. Kelly, T.C. Hufnagel, K. Fezzaa, M.R. Zachariah, Reactive sintering: An important component in the combustion of nanocomposite thermites, *Combust Flame* 159 (2012) 2-15. <https://doi.org/10.1016/j.combustflame.2011.07.015>.
- [22] G.Q. Jian, S. Chowdhury, K. Sullivan, M.R. Zachariah, Nanothermite reactions: Is gas phase oxygen generation from the oxygen carrier an essential prerequisite to ignition?, *Combust Flame* 160 (2013) 432-437. <https://doi.org/10.1016/j.combustflame.2012.09.009>.
- [23] B. Julien, J. Cure, L. Salvagnac, C. Josse, A. Esteve, C. Rossi, Integration of Gold Nanoparticles to Modulate the Ignitability of Nanothermite Films, *Acs Appl Nano Mater* 3 (2020) 2562-2572. <https://doi.org/10.1021/acsanm.9b02619>.
- [24] L. Glavier, A. Nicollet, F. Jouot, B. Martin, J. Barberon, L. Renaud, C. Rossi, Nanothermite/RDX-Based Miniature Device for Impact Ignition of High Explosives, *Propell Explos Pyrot* 42 (2017) 307-316. <https://doi.org/10.1002/prop.201600154>.
- [25] V. Baijot, L. Glavier, J.M. Ducere, M.D. Rouhani, C. Rossi, A. Esteve, Modeling the Pressure Generation in Aluminum-Based Thermites, *Propell Explos Pyrot* 40 (2015) 402-412. <https://doi.org/10.1002/prop.201400297>.
- [26] A. Nicollet, L. Salvagnac, V. Baijot, A. Estève, C. Rossi, Fast circuit breaker based on integration of Al/CuO nanothermites, *Sens Actuat a-Phys* 273 (2018). <https://doi.org/10.1016/j.sna.2018.02.044>.

- [27] T. Wu, F. Sevely, B. Julien, F. Sodre, J. Cure, C. Tenailleau, A. Esteve, C. Rossi, New coordination complexes-based gas-generating energetic composites, *Combust Flame* 219 (2020) 478-487. <https://doi.org/10.1016/j.combustflame.2020.05.022>.
- [28] P. Pennarun, C. Rossi, D. Esteve, D. Bourrier, Design, fabrication and characterization of a MEMS safe pyrotechnical igniter integrating arming, disarming and sterilization functions, *J Micromech Microeng* 16 (2006) 92-100. <https://doi.org/10.1088/0960-1317/16/1/013>.
- [29] B. Larangot, C. Rossi, T. Camps, A. Berthold, P. Pham, D. Briand, M. Puig-Vidal, P. Miribel, D. Esteve, N.D. Rooij, E. Montanes, G. Macias, J. Samitier, Solid Propellant Micro Rockets - Towards a New Type of Power MEMS in: AIAA (Ed.) NanoTech 2002 - "At the Edge of Revolution" Houston, Texas, 2002.
- [30] H.Q. Nie, H.Y. Chan, S. Pisharath, H.H. Hng, Combustion characteristic and aging behavior of bimetal thermite powders, *Def Technol* (2020). <https://doi.org/10.1016/j.dt.2020.05.009>.
- [31] C. Wang, J. Xu, Y. Shen, Y. Wang, T. Yang, Z. Zhang, F. Li, R. Shen, Y. Ye, Thermodynamics and performance of Al/CuO nanothermite with different storage time, *Def Technol* (2020). <https://doi.org/10.1016/j.dt.2020.05.003>.
- [32] P. Simon, Isoconversional methods - Fundamentals, meaning and application, *J Therm Anal Calorim* 76 (2004) 123-132. <https://doi.org/10.1023/B:JTAN.0000027811.80036.6c>.
- [33] B. Roduit, L. Xia, P. Folly, B. Berger, J. Mathieu, A. Sarbach, H. Andres, M. Ramin, B. Vogelsanger, D. Spitzer, H. Moulard, D. Dilhan, The simulation of the thermal behavior of energetic materials based on DSC and HFC signals, *J Therm Anal Calorim* 93 (2008) 143-152. <https://doi.org/10.1007/s10973-007-8864-3>.
- [34] H.E. Kissinger, Reaction Kinetics in Differential Thermal Analysis, *Anal Chem* 29 (1957) 1703-1706. <https://doi.org/10.1021/ac60131a045>.

- [35] G. Lahiner, J. Zappata, J. Cure, N. Richard, M. Djafari-Rouhani, A. Esteve, C. Rossi, A redox reaction model for self-heating and aging prediction of Al/CuO multilayers, *Combust Theor Model* 23 (2019) 700-715. <https://doi.org/10.1080/13647830.2019.1584336>.
- [36] A. Esteve, G. Lahiner, B. Julien, S. Vivies, N. Richard, C. Rossi, How Thermal Aging Affects Ignition and Combustion Properties of Reactive Al/CuO Nanolaminates: A Joint Theoretical/Experimental Study, *Nanomaterials* 10 (2020). <https://doi.org/10.3390/nano10102087>.
- [37] S. Vyazovkin, A.K. Burnham, J.M. Criado, L.A. Perez-Maqueda, C. Popescu, N. Sbirrazzuoli, ICTAC Kinetics Committee recommendations for performing kinetic computations on thermal analysis data, *Thermochim Acta* 520 (2011) 1-19. <https://doi.org/10.1016/j.tca.2011.03.034>.
- [38] I. Abdallah, J. Zapata, G. Lahiner, B. Warot-Fonrose, J. Cure, Y. Chabal, A. Esteve, C. Rossi, Structure and Chemical Characterization at the Atomic Level of Reactions in Al/CuO Multilayers, *ACS Applied Energy Materials* 1 (2018) 17-62. <https://doi.org/10.1021/acsaem.8b00296>.
- [39] H.L. Friedman, Kinetics of thermal degradation of char-forming plastics from thermogravimetry. Application to a phenolic plastic, *Journal of Polymer Science Part C* 6 (1964) 183-195. <https://doi.org/10.1002/polc.5070060121>.
- [40] E.L. Dreizin, Experimental study of stages in aluminum particle combustion in air, *Combust Flame* 105 (1996) 541-556. [https://doi.org/10.1016/0010-2180\(95\)00224-3](https://doi.org/10.1016/0010-2180(95)00224-3).
- [41] D. Stamatis, A. Ermoline, E.L. Dreizin, A multi-step reaction model for ignition of fully-dense Al-CuO nanocomposite powders, *Combust Theor Model* 16 (2012) 1011-1028. <https://doi.org/10.1080/13647830.2012.694480>

- [42] K. Sullivan, M.R. Zachariah, Simultaneous Pressure and Optical Measurements of Nanoaluminum Thermites: Investigating the Reaction Mechanism, *J Propul Power* 26 (2010) 467-472. <https://doi.org/10.2514/1.45834>.
- [43] L. Glavier, G. Taton, J.M. Ducere, V. Bajjot, S. Pinon, T. Calais, A. Esteve, M.D. Rouhani, C. Rossi, Nanoenergetics as pressure generator for nontoxic impact primers: Comparison of Al/Bi₂O₃, Al/CuO, Al/MoO₃ nanothermites and Al/PTFE, *Combust Flame* 162 (2015) 1813-1820. <https://doi.org/10.1016/j.combustflame.2014.12.002>.
- [44] T. Wu, M.R. Zachariah, Silver ferrite: a superior oxidizer for thermite-driven biocidal nanoenergetic materials, *Rsc Adv* 9 (2019) 1831-1840. <https://doi.org/10.1039/c8ra08997c>.
- [45] R.J. Jacob, K.J. Hill, Y. Yang, M.L. Pantoya, M.R. Zachariah, Pre-stressing aluminum nanoparticles as a strategy to enhance reactivity of nanothermite composites, *Combust Flame* 205 (2019) 33-40. <https://doi.org/10.1016/j.combustflame.2019.03.024>.
- [46] R.K. Walzel, V.I. Levitas, M.L. Pantoya, Aluminum particle reactivity as a function of alumina shell structure: Amorphous versus crystalline, *Powder Technol* 374 (2020) 33-39. <https://doi.org/10.1016/j.powtec.2020.06.084>.